Thermoregulated Gas Transport through Electrospun Nanofiber Membranes

Sangil Han[1,2,*] and Gregory C. Rutledge[1]

1 Department of Chemical Engineering, Massachusetts Institute of Technology,

Cambridge, MA 02139, USA

2 Department of Chemical Engineering, Changwon National University,

Changwon 641-773, Korea

* Corresponding author

Tel: +82) 55-213-3757
Fax: +82) 55-283-6465
E-mail address: sangilh@changwon.ac.kr

Abstract: Thermoregulation of gas transport using electrospun fiber membranes is demonstrated experimentally for the first time. The fiber membranes comprise three layers: a middle layer of electrospun polystyrene sandwiched between two outer layers of electrospun cellulose acetate mat as supports, bonded together by hot pressing. The electrospun polystyrene layer serves as a phase change material that blocks transport of gases though the membrane when the fibers de-vitrify. The membrane exhibited a reduction in oxygen flux at temperatures in excess of 140 °C. Using a blend of polysulfone and polystyrene resulted in an upward shift of the transition temperature to 250 °C. Modeling of transport was performed to estimate the impact of the morphological properties of the membranes such as tortuosity, fiber diameter, and porosity.

Keywords: gas permeation; electrospun mat; diffusion; convection; thermoregulation

Introduction

Electrospinning (Ramakrishna et al., 2005; Rutledge and Fridrikh, 2007) is a technology for the production of submicrometer diameter polymer fibers from polymer solutions or melts using electrostatic forces. Fine polymer jets are ejected from a spinneret or free surface at high voltage and stretched by the action of a "whipping" instability. Solid fibers are collected on a grounded target, resulting in nonwoven fiber mats with remarkable characteristics such as high porosity and large surface area (Pai et al., 2009). Such fiber mats have a variety of potential applications including filtration, tissue scaffolds and medical prostheses (Huang et al., 2003).

Due to their large surface areas and interconnected pore structures, functionalized nonwoven electrospun fiber mats can provide good resistance to hazardous chemicals such as volatile organic compounds and aerosols, while allowing water vapor and other inert gases to pass through, offering breathable protective fabrics and membranes (Gibson et al., 1999). While there are now thousands of studies of electrospun membranes, only a few of these works discuss gas transport properties (Chen et al., 2010; Gibson et al., 1999, 2001; Soukup et al., 2010). It is known that the Darcy permeability of fiber membranes, including electrospun membranes, decreases as the square of the fiber diameter for membranes of comparable porosity, as predicted by the analysis of Happel (Happel, 1959).

There are prior research efforts on thermoresponsive membranes for liquid phase transport, with potential applications in biomedical engineering, drug delivery, and tissue engineering. Thermoresponsive polymers such as poly(N-isopropylacrylamide) (PNIPAM) have been used to control the mean pore size of a membrane by swelling and

de-swelling as the polymer switches between hydrophilic and hydrophobic behavior around 32 °C (Ward and Georgiou, 2011). Ionizable polymers with pK_a's between 3 and 10 have been shown to exhibit pH-responsive behaviors (Ward and Georgiou, 2011). In response to a change in pH, acidic groups like carboxylic or phosphoric acids, or basic groups like amines, change their ionization state, resulting in polymer swelling in an aqueous phase (Schmaljohann, 2006).

In this work, we demonstrate thermoresponsive behavior for gas phase transport using a three-layered electrospun membrane where a phase change in the middle layer (actually, a de-vitrification) permits it to swell into and block the pores of the outer layers. The novel three-layered membranes exhibit a significant reduction in gas flux with increasing temperature. Such composite membranes, composed of a thermoresponsive porous middle layer and thermostable porous outer layers, have potential for application in combustion control, sensors, and controlled gas transport in high temperature applications.

Experimental

Preparation of polymer solutions

Cellulose acetate (CA, M_n = 30,000 g/mol), polystyrene (PS, M_w = 280,000 g/mol), and polysulfone (PSU, M_n = 22,000 g/mol) were purchased from Sigma Aldrich. Reagent grade acetone, dimethylacetamide (DMAC), dimethylformamide (DMF) and ethanol were used as received. In a typical solution, 1 g of CA was dissolved in a mixture of 3.8 g acetone and 1.9 g DMAC by stirring overnight to prepare a 15 wt% solution. Similarly, 1 g of PS or a mixture of 0.7 g PS and 0.3 g PSU were dissolved in 4 g of

DMF by stirring at 50 °C overnight to produce a 20 wt% solution of PS or PS:PSU, respectively.

Electrospinning of membranes

Nonwoven fiber membranes were fabricated by electrospinning using a home-built apparatus as described previously (Shin et al., 2001). The polymer solutions were placed in a 10 ml syringe with a capillary needle of 0.05 cm diameter. A positive potential was applied to the polymer solutions by connecting an electrode of a high voltage power supply (ES30P-5W/SDPM, Gamma High Voltage Research, Inc.) to the metal capillary needle. A grounded electrode was connected to a metal collector wrapped by aluminum foil. The applied voltages were 25 kV for the CA solution and 30 kV for the PS and PS:PSU solutions. The feed rate was controlled at 0.015 ml/min for the CA solution and 0.02 ml/min for the PS and PS:PSU solutions using a syringe pump (Infusion PHD 2000, Harvard Apparatus). The metal collector was placed 19 cm or 26 cm below the capillary needle for the CA solution or for the PS and PS:PSU solutions, respectively. After the fabrication, the electrospun mats were dried in a vacuum oven at 80 °C for 2 hours.

Three-layered Membrane Preparation

To form thee-layered composite membranes, a nonwoven electrospun PS or PS:PSU mat was sandwiched between two electrospun nonwoven CA mats and hot-pressing at 80 °C under 4,000 lbs load for 5 min, as described elsewhere (Mannarino and Rutledge, 2012). Disks (3.7 cm in diameter) were cut from the three-layered membranes and sandwiched between two pieces of aluminum tape (Han and Martin, 2009) having

circular openings to expose an effective membrane area of 0.95 cm^2. Silicone glue (RTV Silicone Gasket Maker, Ultra Copper, Permatex®) was used to seal the three-layered membrane where it contacts the aluminum tape, so that gas transport takes place only through the three-layered membrane itself. The thickness of the three-layered membrane was estimated 0.00014 m ± 25% (n=9) using a micrometer equipped with a ratcher thimble (Mitutoyo Co., Japan).

Oxygen Permeation Experiments

Two types of permeation experiments were performed. In the first type of experiment, a gas mixture was fed to the membrane at 1 atm and zero trans-membrane pressure differential. Components of the feed gas diffused across the membrane and were picked up by a sweep gas of helium, and their concentrations measured by gas chromatography. The resulting transport coefficient determined in this experiment is the binary diffusion coefficient. In the second type of experiment, a gas mixture was fed to the membrane at an elevated pressure with respect to the permeate side of the membrane. In this experiment, components of the feed gas permeate the membrane by a combination of diffusion and viscous flow (convection).

For the diffusion experiments, a mixture of oxygen (7 ml/min) and nitrogen (16 ml/min) (30:70) was used as a feed stream that flows continuously across the membrane during the experiments, as illustrated in Figure 1. A stainless steel porous support with 20 μm pore size and 1.6×10^{-3} m thickness (McMaster Carr Co.) was used to support the membrane. The membrane was sealed in place with silicone O-rings (McMaster Carr Co.). Gas compositions in the permeate stream were measured using a gas

chromatograph (GC) (Shimadzu GC-2014 with TCD detector and Restek Molecular Sieve 5A column) with helium carrier gas. The GC was operated at 35 °C column temperature, 50 °C detector temperature, and 15 ml/min helium carrier gas flow. The entire membrane apparatus was placed in an oven (Blue M Box Furnace, Lindberg), where temperature was controlled to an accuracy of ±0.3%. The inlet gas was preheated by passing through a 3 m coil of 3.2×10^{-3} m diameter stainless steel tubing within the furnace, before entering the membrane holder. A thermocouple (42515-T Type K, Extech) with a contact to the surface of the membrane holder was used to measure accurately the temperature of the membrane. A heating rate of 1.3 °C/min was used from 20 °C up to the transition temperature (approximately 140 °C for CA/PS/CA membrane, and 250 °C for CA/PS:PSU/CA membrane), and then a higher heating rate of 7.6 °C/min was applied, up to 400 °C. The slower heating rate was used to ensure equilibration of the fibers at each temperature up to the transition temperature.

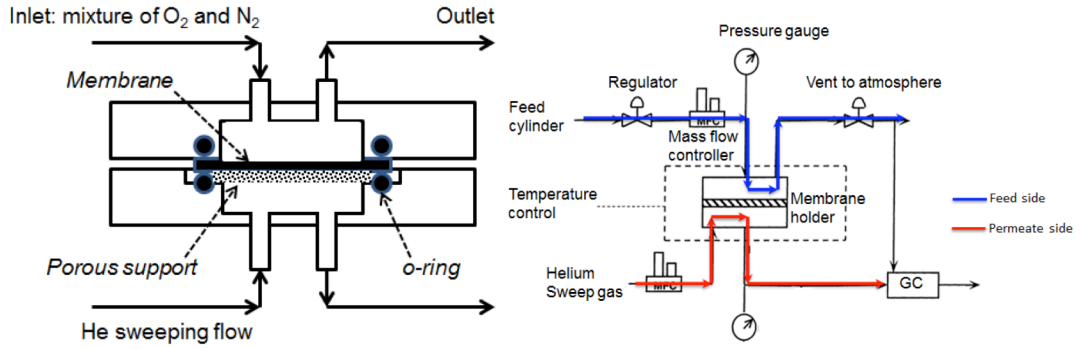

(a) (b)

Figure 1. (a) Schematic of a membrane holder with feed side flow and a permeate side flow. (b) Mixed gas permeability apparatus for gas permeability measurements, adapted from ref. 16.

Diffusive flux and viscous flux measurements and diffusivity calculation

Diffusive flux for oxygen was measured to evaluate the thermoresponsive properties of the porous membranes. Flux J_i was calculated using the flow rate of helium sweep (S) gas, oxygen mole fraction (x_i), and effective membrane area (A): $J_i = x_i S/A$. According to Fick's law (Han and Martin, 2009; Treybal, 1980), $J_i = -D_i \Delta c_i / \ell$; the diffusivity D_i *f*or component *i* was then calculated from the flux J_i, concentration gradient across the membrane in mol/m^2/s, and the membrane thickness, ℓ.

Viscous flux was measured under an applied total pressure of 620 Pa with zero concentration gradient across the CA/PS/CA membrane at 20 °C. In the permeation system of Figure 1(b), the feed side outlet was closed so that the feed gas flows through the membrane under an applied pressure. Gas flow rate on the permeate side was measured using a flow meter (ProFLOW 6000, Restek) with an accuracy of 0.1 ml/min. The pressures on the feed side and the permeate side were measured using two pressure gauges (DPG2001B-15G, Omega) with an accuracy of 68 Pa. The pressure difference across the membranes was controlled by changing the flow rate on the feed side.

Results and Discussion

Membrane characterization

SEM images in Figure 2 show the porous membrane structures for the electrospun CA, PS, and PS:PSU membranes. The fiber diameters were estimated using the ImageJ software (Schneider et al., 2012). The mean fiber diameter for the CA mats was 0.29±0.8 μm. By contrast, the mean fiber diameter for the PS and PS:PSU mats were 1.28±0.4 μm and 1.4±0.3 μm, respectively. Membrane porosities were estimated gravimetrically, using published values from Sigma Aldrich for the densities of CA (1.3 g/ml), PS (1.047

g/ml), and PSU (1.24 g/ml). The mass-averaged mean fiber diameter for the CA/PS/CA three-layer membrane was calculated based on the known fiber diameters for the CA and PS mats, their respective basis weights, and two CA layers per PS layer (resulting in a 3:1 PS/CA mass ratio).

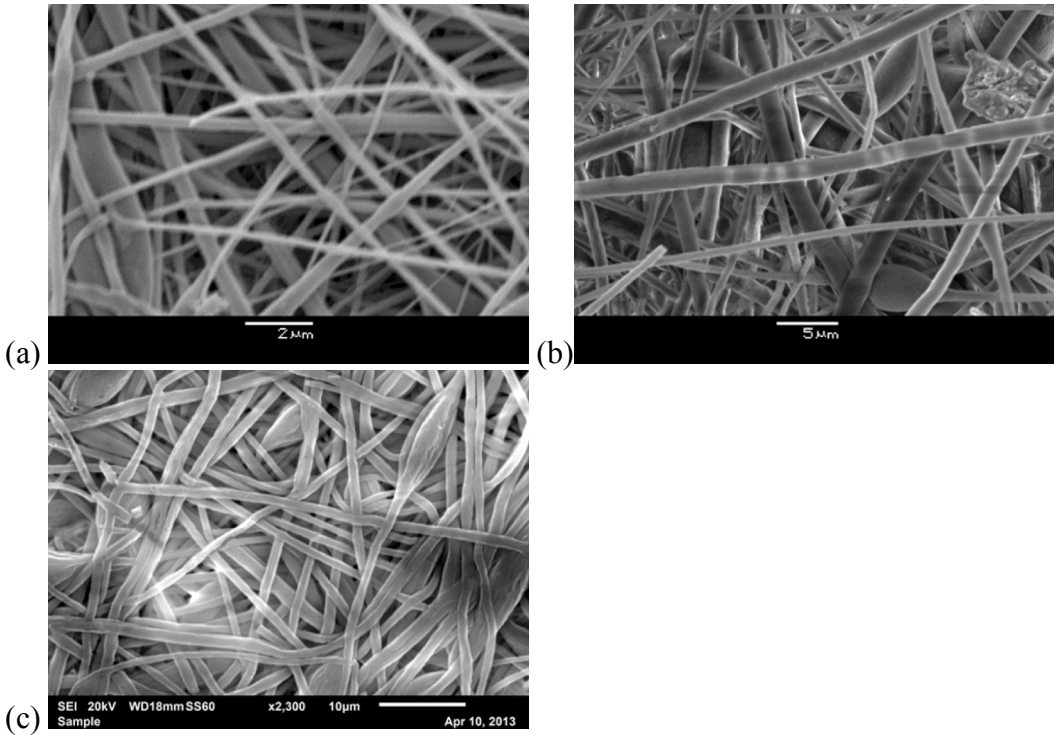

Figure 2. Scanning electron micrographs (SEM) for electrospun mats of (a) cellulose acetate; (b) polystyrene; and (c) PS:PSU (70:30) blend.

(a) 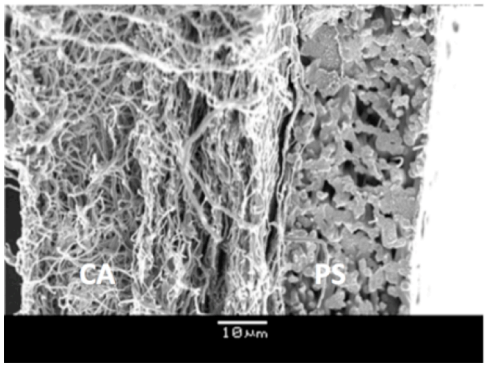

(b) 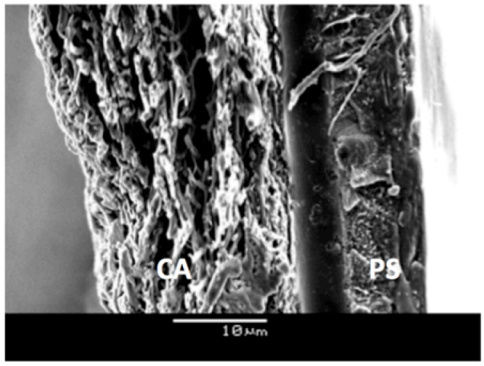

Figure 3. Cross-sectional SEM images for the CA/PS membrane (a) before heating and (b) after heating to 180 °C.

Samples of the membranes were heated to 180 °C for 10 min to verify melting of the fibers. The SEM images in Figures 3 and 4 show that the PS fibers melted while the CA fibers remained unchanged from their original structure. The distinct layer of the PS membrane in the interface between the CA and PS membranes was observed, which might affect the transport properties when fibers were melted. Thermal gravimetric analysis was performed to identify decomposition temperatures for the electrospun mats. The CA fibers decomposed at about 300 °C (supporting information S1), which is lower than the observed decomposition temperatures for either PS (400 °C) or PSU (500 °C) fibers. The 70% mass loss at 400 °C for the PS:PSU mat corresponds to the decomposition of the 70% composition by mass of the PS in the composite of PS and PSU.

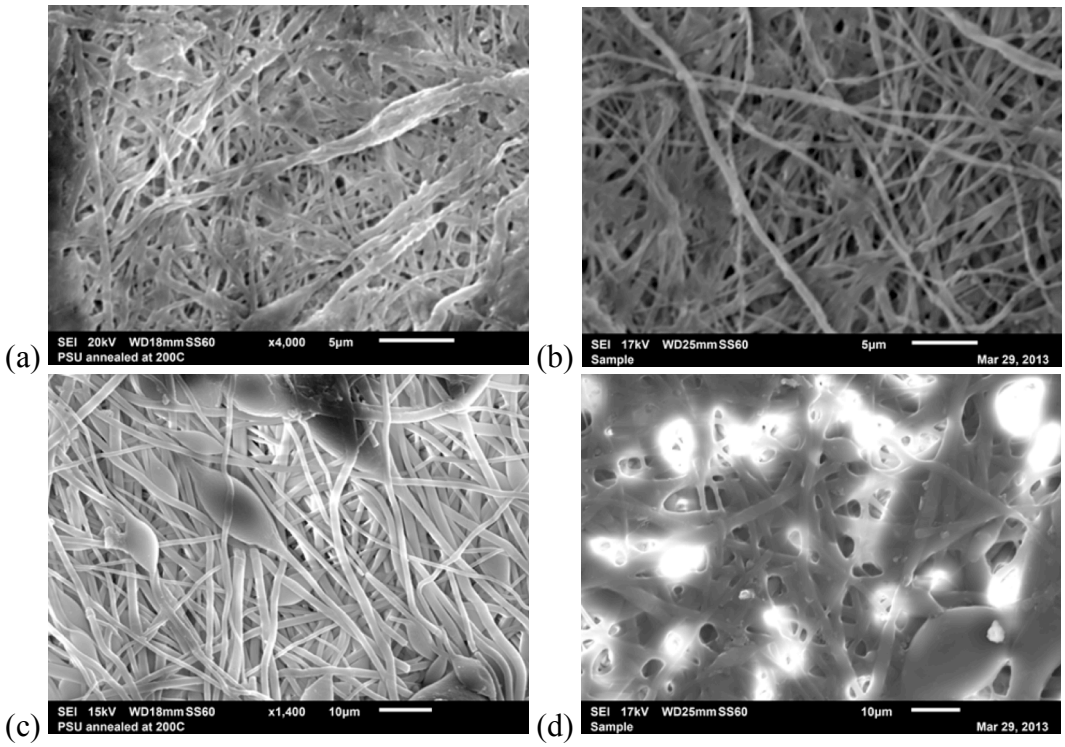

Figure 4. SEM images for a CA/PS bilayer membrane. (a) CA side before heating to 180 °C ; (b) CA side after heating to 180 °C; (c) PS side before heating to 180 °C; (d) PS side after heating to 180 °C

Oxygen permeation in CA and PS electrospun mats

Single layer electrospun CA and PS mats were prepared separately for oxygen permeation experiments. Under a concentration gradient with zero total pressure gradient, the diffusive flux was measured through the electrospun mats as a function of temperature; the results are shown in Figure 5. The flux data in three replicates were obtained after equilibrating for 30 minutes at each temperature. The PS mat showed decreased flux at 150 °C due to the reduced porosity by melting of the fibers; however the decreased flux did not persist, presumably due to lack of support for the liquid film that formed. There was no noticeable flux change in the CA electrospun mat in response to the temperature increase over the range of temperatures tested (20-250 °C).

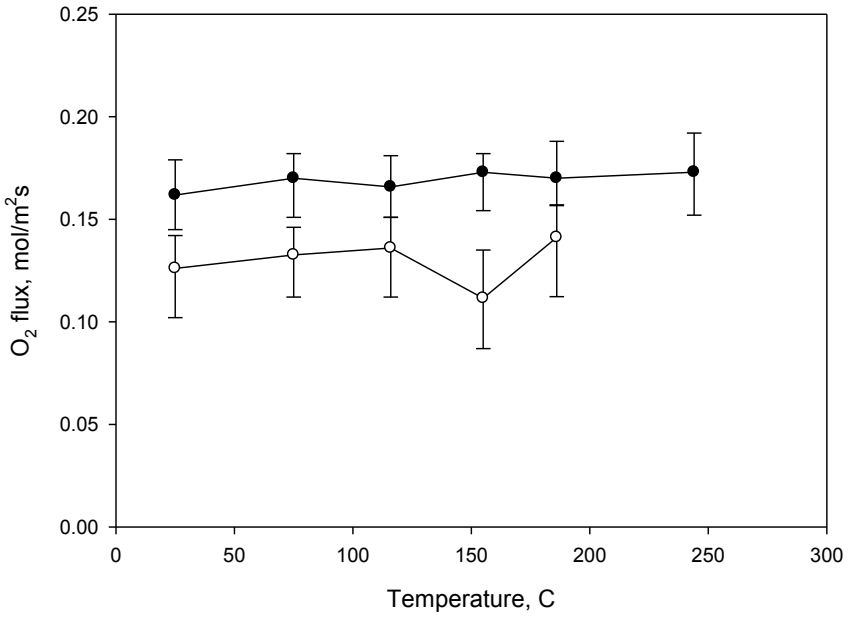

Figure 5. Diffusive flux of oxygen through CA (filled circles) and PS (open circles) single layer electrospun mats. The lower and upper limits of the error bars correspond to minimum and maximum values observed, while the symbol marks the average value (n=3).

Temperature responsive three-layered mat

To address the lack of mechanical integrity of the molten PS film at high temperature and to develop a temperature-responsive membrane that maintains a reduced gas flux at elevated temperatures, the PS mat was sandwiched between two CA mats as supports; the small pore size of the electrospun CA membrane was expected to be beneficial for retaining the molten PS in place at high temperature. The three-layered mats were installed in the membrane permeation cell and the flux was measured in triplicate after 30 min equilibration time at each temperature, up to 280 °C. As shown in Figure 6(a) where the lower and upper limits of the error bars correspond to minimum and maximum values observed, while the closed symbol is the average value (n=3), no

significant decrease in flux was observed from 20 to 130 °C, during which the PS fibers remained intact over the temperature range. With further heating above 130 °C, the flux decreased gradually at first, followed by a significant reduction around 200 °C. The three-layered membrane then maintained the reduced flux values without any compromise of the membrane or the molten PS layer up to 300 °C, at which point the CA fiber mats begin to decompose.

To demonstrate the applicability of the three-layered membrane for gas flux reduction under continuous heating, the transient oxygen flux under steady heating conditions was also measured. Comparing the fluxes and temperatures plotted versus time in Figure 6(b) with the steady state data in Figure 6(a), it appears that the flux begins to decline in both cases when the membrane exceeds 140 °C, but the decline in the transient flux lags that of the steady state flux between 140 and 250 °C. The transient flux values of the Figure 6(b) are larger than the steady state values of the Figure 6(a) during the melting of the fibers. This suggests that the response time for the thermally-induced change in oxygen flux is at least on the order of minutes

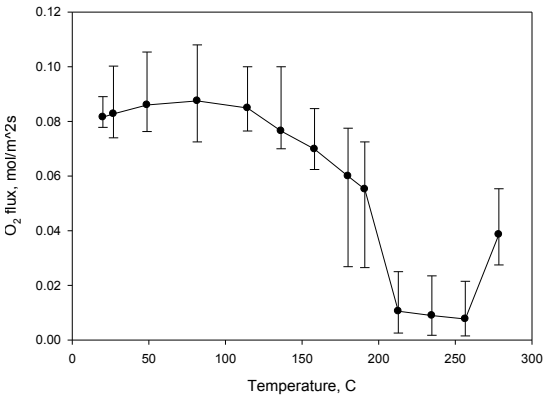

(a)

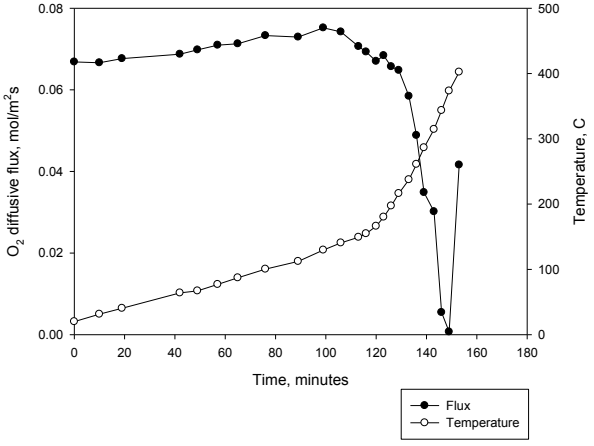

(b)

Figure 6. Oxygen flux though three-layered CA/PS/CA membranes. (a) Steady state diffusive flux of oxygen as a function of increasing temperature. (b) Temperature and oxygen diffusive flow flux as a function of time in a transient heating experiment.

Control of the flux transition temperature using PS:PSU blend

To demonstrate the ability to design for a certain transition temperature at which the flux declines, the PS mid-layer was replaced with a PS:PSU blend mid-layer. PSU was selected because it has a higher glass transition temperature than PS (Lisa et al., 2003) (T_g: 100 °C for PS and T_g: 190 °C for PSU from Sigma Aldrich) due to the strong

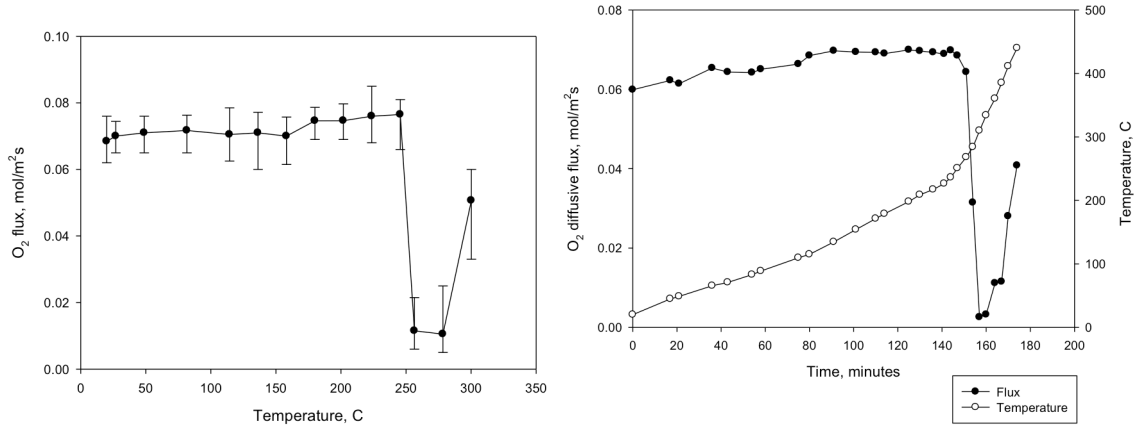

(a) (b)

Figure 7. Oxygen flux though three-layered CA/PS:PSU/CA membranes. (a) Steady state oxygen diffusive flux as a function of increasing temperature. The lower and upper limits in the error bars correspond to minimum and maximum values (n=3). (b) Temperature and oxygen diffusive flux as a function of time in a transient heating experiment.

resonant aryl-sulfone groups. In addition, PSU has been used as an additive for flame retardant materials due to its high thermal stability (Macocinschi et al., 2002). Figure 7(a) shows that the flux transition temperature was increased to 250 °C in the CA/PS:PSU/CA, compared to 140 °C for the CA/PS/CA membranes due to the enhanced thermal stability of the PS:PSU blend. There was no flux reduction in the transient flux measurements up to 250 °C (Figure 7(b)). At 260 and 280 °C, reduced flux was observed. Upon further heating, the flux again increased at around 300 °C, the decomposition temperature of the CA support membranes. The temperature range (250 to 300 °C) for the maximum flux reduction was smaller than the CA/PS/CA membrane (200 to 300 °C).

Diffusive flux analysis for the CA/PS/CA membrane

Transport through a porous medium occurs through the mechanism of diffusion in the presence of a concentration gradient, or convection in the presence of a total pressure gradient. Furthermore, diffusion may be either in the Knudsen regime or the ordinary diffusion regime, depending on the pore size and the mean free path of the gas. The Knudsen number is $Kn = \lambda / L$, where λ is the mean free path and L is the characteristic pore size. For the CA/PS/CA membrane, the pore diameter was estimated to be 2.1 μm, based on a porosity of 62%, fiber diameter of 1.05 μm and the theoretical relation of Sampson for mean pore radius as a function of fiber diameter and porosity (Sampson, 2003). The mean free path at 20 °C and 1 atm was calculated using Eq. 1 to be 0.0673 μm.

$$\lambda = \frac{RT}{\sqrt{2}\pi d^2 N_A P} \qquad \text{(Eq. 1)}$$

where R is the gas constant, d is molecular diameter (3.43 Å for O_2)and N_A is Avogadro's number. Based on these values, the Knudsen number is 0.03, so that ordinary diffusion is the dominant mechanism for diffusion in this work.

In order to calculate the effective binary diffusive flux in the porous membrane structure, where counter-diffusion of helium from the sweep gas on the permeate side occurs across the membrane, the binary mixture diffusion equation (Eq. 2) (Kast and Hohenthanner, 2000) was used. Combining Eq. 2 and Eq. 3, the effective binary diffusivity in a porous medium, D_{12}, is calculated using the diffusivity, D_{exp}, obtained from the flux data at 20 °C in Figure 6.

$$N_{1,dif} = \frac{-D_{12}c}{1-y_1(1+\alpha)}\frac{dy_1}{dx} \quad \text{(Eq. 2)}$$

$$N_{1,dif} = -D_{\exp}c\frac{dy_1}{dx} \quad \text{(Eq. 3)}$$

where $N_{1,\,dif}$ is the diffusive flux for component 1, D_{12} is the effective binary diffusivity in a porous medium, c is the molar density, y_1 is the mole fraction of component 1, x is the position across the membrane, and α = -2.83 is the separation factor, defined as the negative of the square root of the ratio of the molecular weights of the co-diffusing gases (O_2 and He) (Kast and Hohenthanner, 2000). Since the data in Figure 6 is for a composite, three-layered membrane, the experimental diffusivity and the effective binary diffusivity are values characteristic of the entire composite membrane structure.

From the relation between the effective diffusivity D_{12}, binary diffusivity in free space δ_{12}, tortuosity τ and porosity ϕ for a porous medium, expressed by Eq. 4, an estimate of tortuosity was obtained. The binary diffusivity of O_2 and He in free space at 20 °C and 1 atm is δ_{12} =0.736x10^{-4} m^2/s (Wasik and McCulloh, 1969), while the porosity of the three-layered membranes was estimated to be 62%.

$$D_{12} = \frac{\phi\delta_{12}}{\tau} \quad \text{(Eq. 4)}$$

The measured value of D_{exp}=1.84x10^{-6} m^2/s (*c.f.* Eq 3 and Figure 6) is within a factor of four of similar measurements for the diffusivity of water vapor through electrospun polyacrylonitrile fiber membranes (Chen et al., 2010). From this value of D_{exp}, a value for D_{12}=2.62x10^{-6} m^2/s is obtained, which implies a tortuosity of 17. This value is unusually large; tortuosities for electrospun membranes are believed to be close to unity. Likely

sources of error in this analysis are the nonuniformity of membrane thickness, and the complex, non-cylindrical pore geometry of the electrospun fiber membrane.

Viscous flux analysis for the CA/PS/CA membrane

By combination of the viscous flux (Eq. 5) (Lawson and Lloyd, 1997) and the membrane geometry constant B_0 (Eq. 6), the membrane pore radius can be estimated from the ratio of porosity to tortuosity obtained from the diffusive flux analysis.

$$N_{O2,}{}^{V} = \frac{-p_{O2}B_0}{RT\mu}\nabla P \qquad \text{(Eq. 5)}$$

$$B_0 = \frac{\phi r^2}{8\tau} \qquad \text{(Eq. 6)}$$

where $N_{O2}{}^{V}$ is viscous flux, p_{O2} is partial pressure of oxygen, μ is air viscosity (1.83×10^{-5} kg/s·m), P is total pressure, r is pore radius, ϕ is porosity, τ is tortuosity. From an oxygen flux of 0.193 mol/m^2/s measured at 824 Pa of trans-membrane pressure differential for the CA/PS/CA membrane, Eq. 5 yields a value for $B_0 = 4.51\text{x}10^{-14}$ m^2, from which the estimated pore diameter is 8.49 μm, by Eq 6. This estimated diameter is four times larger than the calculated pore diameter of 2.1 μm from Sampson's theory. The deviation might be due to the inaccuracy of the estimation for the nominal diameters in the CA/PS/CA three-layered membrane.

Conclusions

Performance measurements on the three-layered membranes shows that the thermoresponsive transport performance for gas flux can be realized using a three-layer composite membrane design. Flux of oxygen through the membranes was more or less

constant up to a transition temperature of 140 °C for the CA/PS/CA membranes, or 240 °C for the CA/PS:PSU/CA membranes. The transition temperature is determined primarily by the glass transition temperature of the thermoresponsive (middle layer) component. For temperatures above the transition temperature, oxygen flux was reduced by as much as 8-fold. The response time of the thermally induced reduction in gas flux is on the order of minutes, based on the lag in flux reduction in transient heating experiments, compared to steady state experiments. The three-layered membranes effectively maintained reduced oxygen flux up to 300 °C, at which point decomposition of the CA component led to failure of the membrane. Control of the flux transition temperature was shown by blending PSU with PS, resulting in shifting of the transition temperature from 140 to 240 °C. This simple modification technique demonstrates a method for designing the thermoresponsive membranes for different applications, depending on the thermal properties of fibers.

Both diffusive flux measurements with a concentration gradient and viscous flux measurements under a total pressure gradient were performed to characterize membrane geometry. The binary diffusive flux model, $N_{1,\,diff}$, and the effective binary diffusivity, D_{12}, were combined to estimate a ratio of porosity to tortuosity for the CA/PS/CA membrane. The viscous flux equation was used to estimate the pore diameter of the CA/PS/CA membrane using the obtained ratio of porosity to tortuosity. To our knowledge, this is the first demonstration of a thermoresponsive membrane that exhibits a reduction in gas flux above a defined transition temperature. Further work should be performed to discover potential applications such as gas sensing, combustion control, and temperature responsive gas filtration.

Acknowledgement

The authors are grateful to Philip Morris International for financial support of this work.

References

Chen, L., Bromberg, L., Lee, J.A., Zhang, H., Schreuder-Gibson, H., Gibson, P., Walker, J., Hammond, P.T., Hatton, T.A., Rutledge, G.C., 2010. Multifunctional electrospun fabrics via layer-by-layer electrostatic assembly for chemical and biological protection. Chem. Mater. 22, 1429-1436.
Gibson, P.W., Schreuder-Gibson, H.L., Rivin, D., 1999. Electrospun fiber mats: Transport properties. AIChE J. 45, 190-195.
Gibson, P.W., Schreuder-Gibson, H.L., Rivin, D., 2001. Transport properties of porous membranes based on electrospun nanofibers. Colloids Surf. A 187–188, 469–481.
Han, S., Martin, S.M., 2009. Diffusivity and solubility of organic solutes in supported liquid crystal membranes. J. Phys. Chem. B 113, 12696–12703.
Happel, J., 1959. Viscous flow relative to arrays of cylinders. 5, 174-177.
Huang, Z., Zhang, Y.Z., Kotaki, M., Ramakrishna, S., 2003. A review on polymer nanofibers by electrospinning and their applications in nanocomposites. Comp. Sci. Tech. 63, 2223-2253.
Kast, W., Hohenthanner, C.R., 2000. Mass transfer within the gas-phase of porous media. Inter. J. Heat Mass Transfer 43, 807-823.
Lawson, K.W., Lloyd, D.R., 1997. Membrane distillation. J. Mem. Sci. 124, 1-25.
Lisa, G., Avram, E., Paduraru, G., Irimia, M., Hurduc, N., Aelenei, N., 2003. Thermal behaviour of polystyrene, polysulfone and their substituted derivatives. Polym. Deg. Stab. 82, 73-79.
Macocinschi, D., Grigoriu, A., Filip, D., 2002. Aromatic polysulfones for flame retardancy. Europ. Polym. J. 38, 1025-1031.
Mannarino, M.M., Rutledge, G.C., 2012. Mechanical and tribological properties of electrospun PA 6(3)T fiber mats. Polymer 53, 3017-3025.
Pai, C., Boyce, M.C., Rutledge, G.C., 2009. Morphology of Porous and Wrinkled Fibers of Polystyrene Electrospun from Dimethylformamide. 42, 2102-2114.
Ramakrishna, S., Fujihara, K., Teo, W.E., Lim, T.C., Ma, Z., 2005. An Introduction to Electrospinning and Nanofibers. World Scientific: Singapore.
Rutledge, G.C., Fridrikh, S.V., 2007. Formation of fibers by electrospinning. Adv. Drug Deliv. Rev. 59, 1384-1391.
Sampson, W.W., 2003. A multiplanar model for the pore radius distribution in isotropic near-planar stochastic fibre networks. J. Mater. Sci. 38, 1617-1622.
Schmaljohann, D., 2006. Thermo- and pH-responsive polymers in drug delivery. Adv Drug Deliv Rev 58, 1655-1670.
Schneider, C.A., Rasband, W.S., Eliceiri, K.W., 2012. NIH Image to ImageJ: 25 years of image analysis. Nat. Methods 9, 671-675.

Shin, Y.M., Hohman, M.M., Brenner, M.P., Rutledge, G.C., 2001. Experimental characterization of electrospinning: the electrically forced jet and instabilities. Polymer 42, 09955-09967.
Soukup, K., Petráš, D., Klusoň, P., Šolcová, O., 2010. Nanofiber membranes—Evaluation of gas transport. Catal. Today 156, 316-321.
Treybal, R.E., 1980. Mass-Transfer Operations. McGraw-Hill.
Ward, M.A., Georgiou, T.K., 2011. Thermoresponsive polymers for biomedical applications. Polymers 3, 1215-1242.
Wasik, S.P., McCulloh, K.E., 1969. Measurements of gaseous diffusion coefficients by a gas chromatographic technique. J. Res. Natl. Bur. Stand. Sec. A 73A, 207-211.